ChemComm

Recovery of Xenon from Air over ZIF-8 Membranes

Journal:	*ChemComm*
Manuscript ID	CC-COM-05-2018-004154.R1
Article Type:	Communication

Journal Name

COMMUNICATION

Recovery of Xenon from Air over ZIF-8 Membranes

Ting Wu, [a] Jolie Lucero, [a] Michael A. Sinnwel, [b] Praveen K. Thallapally,* [b] and Moises A. Carreon* [a]

Received 00th January 20xx,
Accepted 00th January 20xx

DOI: 10.1039/x0xx00000x

www.rsc.org/

Continuous ZIF-8 membranes effectively separated air/Xe gas mixtures. These membranes showed air permeances as high as 3.94 x 10^{-8} mol/m^2 s Pa and separation selectivities as high as 12.4 for air/Xe molar feed composition of 9:1. These membranes separated air from Xe via molecular sieving, preferential adsorption, and diffusivity differences.

Xenon (Xe) is an expensive and important inert gas for many medical and commercial applications. Xe is used in lighting, electrical, aerospace, and medical applications.[1] In lighting industry, it is used primarily in photographic flash lamps, [1a] arc-lamps in plasma display panels [1b] solar simulation, [1c] and blue headlights and ant-fog lights on vehicles/as automotive lightings.[1d] As an easily-ionized inert gas with high atomic mass and cryogenic storage density, Xe is the most popular propellant used in ion thrusters for satellites in the aerospace field.[1e] Xe is also used as a nontoxic anesthetic[1f] and scintillator and ionization-chamber material in X-ray for medical imaging applications. [1g]

The widespread use of Xe gas appears even more remarkable when its cost is considered. Xe costs about $262 for 11 liters at market rates.[2] A decrease in market price for high quality Xe would benefit the medical and commercial industries, as well as promote the development of new Xe applications. The high cost of Xe gas derives from the current energy- and capital- intensive cryogenic distillation separation process of air, and the low concentration of Xe in air, which is only 0.086 ppm.[1f] Cryogenic distillation requires cooling air below the boiling points of nitrogen and oxygen (N_2: -196˚C, O_2: -183˚C, Xe: -108˚C) [3] to separate the inert gas from the mixture. In a typical cryogenic air separation plant, intensive capital and energy costs are expended in a series of process units that involve air compression, air purification, heat exchanging, distillation, and product compression.[4] Because this process is so expensive, very little Xe is separated from air. Yearly world production Xe amounts to just 80.7 metric tonnes (14 million liters) per year while Earth's atmosphere contains 2 billion tonnes.[5]

Several adsorbents have been proposed to recover Xe from air as a potentially cheaper production method.[6] This technology relies on the adsorption capacity difference between Xe atoms and other atoms and molecules in air rather than on phase change differences. In most of these reports, carbon, zeolite and metal organic frameworks (MOFs) have been used to capture noble gases from air.[6b-e] Shino et al. reported an approach to produce highly pure Xe by cooling air to liquefy oxygen and using a main condenser filled with an adsorbent to catch Xe condensate.[6a] Golden et al. employed Li- and Ag-exchange zeolites with periodic thermal regeneration as absorbents to recover Xe and Kr from an oxygen-containing gas derived from a liquid oxygen stream in a cryogenic air separation plant.[6b] Bazan et al. studied the adsorption difference between gaseous O_2, Kr, Xe, and Ar over activated carbon and zeolites, finding that Xe was the most strongly adsorbed gas.[6c] Parkes et al. screened MOFs for adsorbing noble gases in air based on the effect of pore sizes and framework topologies.[6d] Specifically, the authors found that some MOFs displayed Xe/N_2 selectivity up to 26:1.[6d] Thallapally et al. demonstrated that a Ni-based MOF denoted as NiDOBDC, displays higher Xe/N_2 adsorption selectivity than activated carbon. [6e]

Although adsorbents for Xe recovery from air are well documented, to our best knowledge, no research related to the recovery of Xe from air based on membrane technology has been reported. In this study, we demonstrate the separation ability of ZIF-8 membranes for recovering Xe from air. ZIF-8 is a metal organic framework displaying a microporous crystalline structure with a sodalite (SOD) topology, formed by connecting zinc ions with nitrogen atoms of 2-methylimidazole.[7] ZIF-8 is a highly suitable candidate to molecular sieve air (N_2 and O_2) over Xe. ZIF-8 has effective pore size range of (0.4–0.42 nm) [8] while the kinetic diameter of

[a] Chemical and Biological Engineering Department, Colorado School of Mines, Golden, CO 80401 United States
Email: mcarreon@mines.edu
[b] Physical & Computational Sciences Directorate, Pacific Northwest National Laboratory, Richland, WA 99352 United States
Email: Praveen.Thallapally@pnnl.gov

† Electronic Supplementary Information (ESI) available. See DOI: 10.1039/x0xx00000x

O_2, N_2 and Xe are ~0.35 nm, ~0.36 nm[9] and 0.41 nm[10] respectively. Therefore, in principle molecular sieving of air over Xe should be expected over ZIF-8 membranes. Furthermore, the lighter weights of O_2 and N_2 (as compared to Xe) should promote faster air molecules diffusion.[11] The molecular sieving properties of ZIF-8 membranes have been demonstrated for several binary gas mixtures.[12] Comprehensive and representative reviews on the progress of MOF membranes for molecular gas separations have been reported.[13]

The separation performance of ZIF-8 membranes prepared in this study was evaluated using premixed air/Xe gas mixtures with molar ratio of 9:1. The feed and permeate pressures were kept at 223 kPa and 85 kPa, respectively. The detailed membrane synthesis and separation methods are described in Supplementary Information (ESI†). The separation data for three ZIF-8 membranes is shown in Table 1. Two membranes **M1** and M2 were synthesized independently via solvothermal approach (Table S1, ESI†). The first layer of membranes **M1** and **M2** was prepared at 120°C for 10 hours. Extended solvothermal synthesis times allow better crystalline intergrowth. We applied two layers for these membranes since one-layer membranes were defective/discontinuous. The second layer of **M1** and **M2** was added over a shorter duration of three and four hours respectively at 120 °C to limit crystal growth and form a continuous layer. **M1** and **M2** displayed permeances of 3.1 and $3.9x10^{-8}$ mol/m^{2}sPa and air**/**Xe separation selectivities of 11.3 and 12.4. Membrane **M3** was prepared by adding an extra ZIF-8 layer to a membrane prepared with identical gel compositions and solvothermal synthesis conditions as those of **M1** to form a 3-layer membrane. Separation selectivity decreased compared to those of the 2-layer membranes (**M1** and **M2**). The reduction in separation selectivity may be associated with an increase in the concentration of defects and/or non-selective pore pathways.

The separation index π was used to assess membrane reproducibility. This index [π= air permeance × (selectivity-1) × permeate pressure] constitutes a reliable parameter to predict porous crystalline membrane reproducibility and evaluate general membrane performance.[14] Membrane separation indexes ranged between 2.1 $x10^{-2}$ and $3.8x10^{-2}$ mol/m^{2}s respectively, indicating good membrane reproducibility.

Table 1 Air (N_2 and O_2) /Xe separation performance over ZIF-8 membranes at room temperature; molar gas mixture composition: 9:1 air/Xe; transmembrane pressure: 138 kPa; feed flow rate: 40 ml/min. Numbers in parenthesis indicate Gas Permeation Units (GPU)

Membrane ID	Air permeance $x10^{-8}$(mol/m2·s·Pa) (GPU)	Separation selectivity (α)	Separation index (π) $x10^{-2}$ (mol/m^2 s)
M1	3.10 (92.6)	11.3	2.7
M2	3.94 (117.7)	12.4	3.8
M3	3.94 (117.7)	7.4	2.1

Representative SEM images of membranes **M1–M3** are shown in Figure 1. Top view SEM images of **M1–M3** (Figures 1a, 1c, 1e) show well-intergrown and interconnected micron-range ZIF-8 crystals. A distinctive morphological feature of membranes **M1**-**M3** is the presence of pyramidal-shaped crystals. We have observed this crystal morphology previously.[12b] This morphology may have resulted from the membrane different solvothermal histories (Table S1, ESI†). In general, membranes **M1** and **M2** show smaller crystal aggregates sized up to ~33 μm as compared to **M3**, which contains aggregates sized up to ~68 μm. **M3**'s larger crystal aggregates may have grown during the recrystallization process upon the addition of the third layer. The cross-sectional image of membrane **M1**, shown in Figure 1b, displays a dense membrane layer with thickness of ~13±3 μm. **M2** shows a slightly thicker layer of ~14±2 μm as shown in Figure 1d. **M3** displayed a thickness of 27±6 μm (Figure 1e). **M2** and **M3** displayed higher air permeance than **M1**. Since these two membranes are thicker than **M1**, this suggests that their higher permeance may be related to a higher concentration of defects. It is common that ZIF-8 polycrystalline membrane performance is highly dependent on microstructure characteristics, including morphology, crystal size, thickness, intergrowth, defects, and gaps or cracks.[12i]

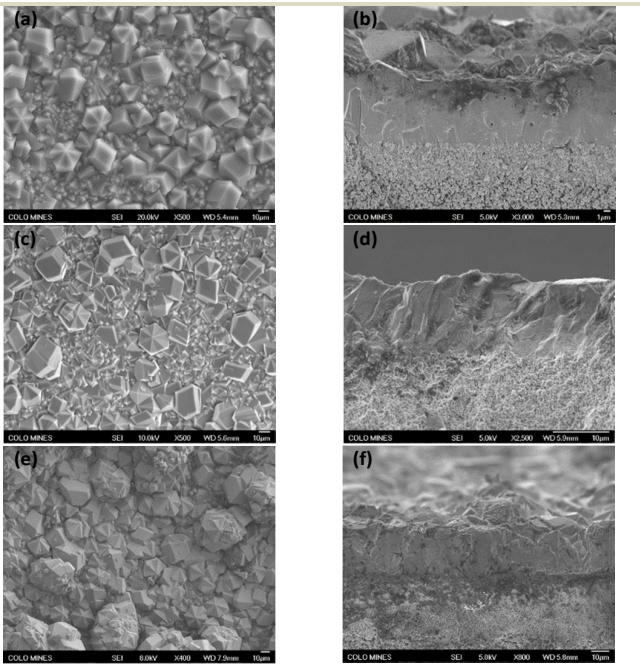

Fig. 1 Representative cross section and top views SEM images of ZIF-8 membranes: (a) and (b) for membrane **M1**; (c) and (d) for membrane **M2**; (e) and (f) for membrane **M3**.

To understand the role of adsorption of N_2 and Xe over ZIF-8, adsorption isotherms were collected for N_2 and Xe. We employed pure N_2 as a reasonable approximation of air composition (79% N_2 in air). Figure 2 shows the single adsorption isotherms for N_2 and Xe measured at 10 °C, and 25°C for ZIF-8 crystals. The isotherms indicate that the Xe/N_2 adsorption selectivity decreases as temperature decreases. Specifically, the Xe/N_2 adsorption selectivity at P/Po = 1, was 9.0 and 4.8 at 25 °C and 10 °C respectively.

The isosteric heats of adsorption (Qst) of Xe and N_2 gases were calculated by Virial method, using the experimental single adsorption isotherms collected at 298 K and 283 K for both gases. ZIF-8 exhibits Qst values for Xe and N_2 of ~-17 and ~-11 kJ/mol, respectively (Figures S2–S3, ESI†). These values indicate Xe preferential adsorption over N_2, a fact attributable to the greater polarizability of Xe molecules. The higher Xe static dipole polarizability (Xe: 25.297-27.42 atomic units; N_2:7.26 atomic units [15]) leads to stronger van der Waals interactions with the -C=C- polar ligand of ZIF-8. Therefore, stronger electrostatic interactions between the ZIF-8 surface and Xe lead to Xe preferential adsorption. The higher Xe adsorption over ZIF-8 indicates that adsorption between Xe and N_2 is a strong competitive separation mechanism.

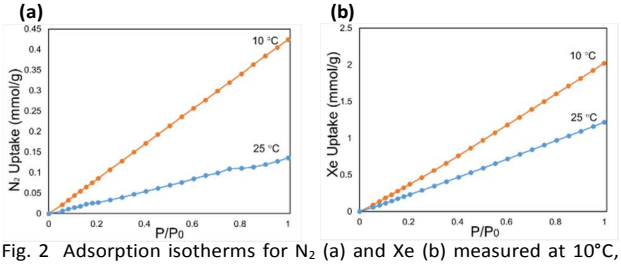

Fig. 2 Adsorption isotherms for N_2 (a) and Xe (b) measured at 10°C, and 25°C for ZIF-8 crystals.

To learn about transport properties of air and Xe over ZIF-8 membranes, effective diffusion coefficients for these gases were estimated using Fickian law, $\boldsymbol{J} = -\boldsymbol{D}\frac{\partial \boldsymbol{C}}{\partial \boldsymbol{d}}$. The calculation process is shown in Table S2 (ESI†). The calculated diffusion coefficients implicitly include adsorption effects since they were derived from membrane experiment measurements. The estimated Fickian diffusivities (Table 2) results indicate that air diffuses faster than Xe through ZIF-8 membranes, and therefore suggesting that difference in diffusivities promotes the separation of air from Xe.

Table 2. Estimated diffusivities for air/Xe gas mixture over ZIF-8 membranes at room temperature.

Membrane ID	Membrane thickness (μm)	Air Diffusivity (m^2/s) x10^{-10}	Xe Diffusivity (m^2/s) x10^{-11}	D(Air)/D(Xe)
M1	13±3	9.7	9.6	10.2
M2	14±2	12.2	12.6	9.7
M3	27±6	25.7	37.4	6.9

Molecular sieving and *differences in diffusivities* were the two main separation mechanisms which contributed to the observed air over Xe selective membranes. The effective aperture size of ZIF-8 (~0.4-0.42 nm), lying between the kinetic diameters of N_2 and O_2 (0.36 nm, and 0.35 nm) and Xe (~0.41 nm), suggests potential molecular sieving properties of ZIF-8 membranes for this gas mixture. Estimation of Fickian diffusivities indicate that air diffuses faster than Xe promoting the separation *via* differences in diffusivities. On the other hand, the observed Xe/air *preferential adsorption selectivity* (Figure 2) competes strongly against molecular sieving and diffusivity differences. The structural framework flexibility of ZIF-8 leads to Xe permeation. This "gate opening functionality" can change the ZIF effective pore aperture helping to promote the separation via differences in diffusivities. This is supported by recent MD simulations which demonstrate that Xe can pass through 0.41 nm ZIF-8 pores.[12d] This pore size is close enough to potentially promote molecular sieving too. The size selective properties of ZIF-8 have been well recognized. [16] Nevertheless, the observed air/Xe separation selectivities indicate that molecular sieving and differences in diffusivities were the two dominant separation mechanisms.

Adsorption isotherms for N_2 and Xe (Figure 2) suggest that the competitive adsorption mechanism can be attenuated if the separation is carried out at lower temperature (since the Xe/N_2 adsorption selectivity decreases with decreasing temperature). Based on this premise, we carried out the separation experiments at 10 °C. As shown in Figure 3, both permeance and separation selectivities slightly increased at 10 °C. Overall, the separation indexes for the ZIF-8 membranes increased by 14%-19%.

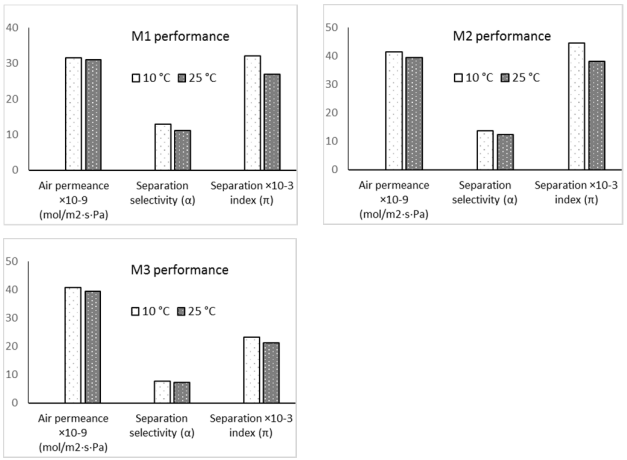

Fig. 3 Air (N_2 and O_2)/ Xe separation performance over ZIF-8 membranes at 10°C and 25°C; molar gas mixture composition: 9:1 air/Xe; transmembrane pressure: 138 kPa; feed flow rate: 40 ml/min.

Table 3 shows the compositions of air (N_2 and O_2) and Xe in the permeate, feed, and retentate streams. Overall, the three membranes showed effective Xe recovery. There was a marked difference in retentate and feed compositions. As Table 3 shows, the permeate compositions of air increased by ~8%-9% and those of Xe decreased by 74%-84%. The retentate compositions of air decreased by only ~1%-2% and those of Xe increased by 13%-22%. The retentate gas composition changed only marginally due to the lower permeate flow rate versus retentate flow rate. If the retentate flow were collected and repeatedly recycled through the separation system, in principle Xe recovery would increase.

Table 3. Air and Xe compositions and change percentages in permeate and retentate flows for air/Xe mixture at room temperature; molar gas mixture composition: 9:1 air/Xe. Transmembrane pressure: 138 kPa. Parenthesis indicate the composition change percentage (+/-) compared to that in the feed flow.

Membrane	Permeate composition	Retentate composition

ID	Air%	Xe%	Air%	Xe%
M1	98.32 (+9.2%)	1.68 (-83.2%)	88.74 (-1.4%)	11.26 (+12.6%)
M2	98.39 (+9.3%)	1.61 (-83.9%)	87.85 (-2.4%)	12.15 (+21.5%)
M3	97.45 (+8.3%)	2.55 (-74.5%)	87.96 (-2.3%)	12.04 (+20.4%)

In summary, we demonstrate the synthesis of continuous ZIF-8 membranes for the separation of air/Xe gas mixtures. These membranes displayed permeances as high as 3.9 x 10^{-8} mol/m^2 s Pa and separation selectivities as high as 12.4 for air/Xe feed molar compositions of 9:1. Separation mechanisms included molecular sieving, competitive adsorption, and diffusivity differences. The former two mechanisms were dominant leading to air selective membranes. The proposed membrane technology represents a promising alternative to separate Xe from air mixtures. To the best of our knowledge, this report work represents the first example of any porous crystalline membrane displaying separation ability for air /Xe gas mixtures.

This work was supported by the Department of Energy Nuclear Energy University Program under Grant No. DE-NE0008429.

Conflicts of interest

There are no conflicts to declare.

Notes and references

1 (a) A. Wekhof, *PDA J. Pharm. Sci. Tech*. **2000**, *54*, 264; (b) C. H. Kim, I. E Kwon, C. H. Park, Y. J. Hwang, H. S. Bae, B. Y. Yu, G. Y. Hong, *J. Alloys Compd.* **2000**, *311*, 33; (c) S. Ito, H. Matsui, K. Okada, S. Kusano, T. Kitamura, Y. Wada, S . Yanagida, *Sol. Energy Mater Sol. Cell*, **2004**, *82*, 421; (d) K. Eichhorn, *Proc. SPIE*, **2006**, *6134,* 6134051: (e) NASA – Ion Propulsion https://www.nasa.gov/centers/glenn/about/fs21grc.html; (f) N. P. Franks, R. Dickinson, SLM De Sousa, A. C. Hall, W. R. Lieb, *Nature*. **1998**, *396*, 324; (g) C. W. E. Van Eijk, *Phys. Med. Biol*. **2002**, *247*, R85.

2 Sigma Aldrich – Xenon https://www.sigmaaldrich.com/catalog/product/sial/00472?lang=en&region=US

3 Compressed Gas Association*, Handbook of Compressed Gases*; Reinhold Publishing Corporation: New York, NY, **1966**.

4 A. Darde, R. Prabhakar, J. P. Tranier, N. Perrin, *Enrgy. Proced*. **2009**, *1*, 527.

5 R. Betzendahl, *Cryo Gas International,* **2013**, *29*, 32.

6 (a) M. Shino, H. Takano, J. Nakata, U.S. Patent No. 5,039,500. Aug. 13, **1991**; (b) T. C. Golden, T. S. Farris, R. L. Chiang, R. D. Whitley, F. W. Taylor U.S. Patent No. 6,658,894. 9, Dec. **2003**; (c) R. E. Bazan, M. Bastos–Neto, A. Moeller, F. Dreisbach, R. Staudt, *Adsorption*, **2011**, *17*, 371; (d) M. V. Parkes, C. L. Staiger, J. J. Perry IV, M. D. Allendorf, J. A. Greathouse, J. *Phys. Chem. Chem. Phys.* **2013**. *15*, 9093; (e) P. K. Thallapally, J. W. Grate, R. K. Motkuri, *Chem Commun*, **2012**, *48*, 347

7 (a) K. S. Park, Z. Ni, A. P. Côté, J. Y. Choi, R. Huang, F. J. Uribe–Romo, H. K. Chae, M. O'Keeffe, O. M. Yaghi, *P Natl Acad SCI*, **2006**, *103*, 10186; (b) C. Baerlocher, D. H. Olson, W. M. Meier, *Atlas of Zeolite Framework Types;* Elsevier Science & Technology: Netherlands, **2001**.

8 C. Zhang, R. P. Lively, K. Zhang, J. R. Johnson, O. Karvan, W. J. Koros, *J. Phys. Chem. Lett.* **2012**, *3*, 2130.

9 A. F. Ismail, K. C. Khulbe, T. Matsuura, *Gas separation membranes*, **2015**, *7*, 14. Switzerland: Springer. P.14

10 D. W. Breck, *Zeolite Molecular Sieves: Structure, Chemistry and Use*, Jonh Wiley and Sons. Inc., New Ypirk, Malabar, Flórida 1974.

11 J. R. Li, R. J. Kuppler, H. C. Zhou, *Chemical Soc Rew.* **2009**, *38*, 1477.

12 (a) S. R. Venna, M. A. Carreon, *J. Am. Chem. Soc*. **2010**, *132*, 76; (b) T. Wu, X. Feng, S. K. Elsaidi, P. K. Thallapally, M. A. Carreon, *Ind. Eng. Chem. Res.* **2017**, *56*, 1682: (c) T. Wu, J. Lucero, Z. Zong, S. K. Elsaidi, P. K. Thallapally, M. A. Carreon, *ACS Appl. Nano Mater.* **2018**, *1*, 463; (d) R. Anderson, B. Schweitzer, T. Wu, M. A. Carreon, D. A. Gomez–Gualdron, *ACS Appl. Mater. Interfaces*. **2018**, *10*, 582; (e) H. Bux, C. Chmelik, J. M. van Baten, R. Krishna, J. Caro, *Adv. Mater.* **2010**, *22*, 4741; (f) H. Bux, C. Chmelik, R. Krishna, J. Caro, *J. Membr. Sci.* **2011**, *369*, 284; (g) H. Bux, F. Liang, Y. Li, J. Cravillon, M. Wiebcke, J. Caro, *J. Am. Chem. Soc.* **2009**, *131*, 16000; D. Liu, X. Ma, H. Xi, Y. S. Lin, *J. Membr. Sci.* **2014**, *451*, 85; (h) H. T. Kwon, H.–K. Jeong *J. Am. Chem. Soc.* **2013**, *135*, 10763

13 (a) M. Shah, M.C. McCarthy, S. Sachdeva, A.K. Lee, H.-K. Jeong, *Ind Eng Chem Res.* **2011,** *51* , 2179; (b) J. Yao, H. Wang., *Chem Soc Rev*, **2014**, *43*, 4470; (c) S. Qiu, M. Xue, G. Zhu, *Chem Soc Rev*, **2014**, *43*, 6116; (d) S.R. Venna, M.A. Carreon. *Chem Eng Sci* **2015**, *124*, 3; (e) Y.S. Lin. *Current Opinion in Chemical Engineering* **2015**, *8*, 21; (f) Zixi Kang, Lili Fan, Daofeng Sun. *J. Mater. Chem. A* **2017**, *5*, 10073.

14 M. A. Carreon, S. Li, J. L. Falconer, R. D. Noble, *Adv. Mater.* **2008**, *20*, 729

15 (a)A. K. Das A. J. Thakkar, *J. Phys. B, At. Mol. Opt. Phys*. **1998**, *31*, 2215; (b) B. K. Mani, K. V. P. Latha, D. Angom, *Phys. Rev. A* **2009**, *80*, 0625051; (c) V. G. Bezchasnov, M. Pernpointner, P. Schmelcher, L. S. Cederbaum, *Phys. Rev. A* **2010**, *81*, 0625071.

16 (a) X. Wang, C. Chi,J. Tao, Y. Peng,S.Ying,Y. Qian, J. Dong, Z. Hu, Y. Gu, D. Zhao, *Chem. Commun*. **2016**, *52*, 8087; (b) C. Zhang, R. P. Lively, K. Zhang, J. R. Johnson, O. Karvan, W. J. Koros, *J. Phys. Chem. Lett*. **2012**, *3*, 2130.